In-vitro Tumor Mimetic Spheroid Model: Void Space within a Self-detachable Crosslinked Hydrogel

*Narendra Kale, Connor Edvall, Chukwuebuka Ozoude, Sanku Mallik**

Pharmaceutical Sciences Department, North Dakota State University, Fargo, North Dakota 58105, United States.

KEYWORDS: hypoxia, alginate, HIF-1α, CA-9, cancer cell spheroid.

ABSTRACT

The three-dimensional (3D) spheroid cell culture model is crucial in screening anticancer drugs in vitro and understanding tumor cell behavior. However, the current in-vitro models require highly skilled techniques and often lack reproducible results. Here, we present an in-vitro, tumor-mimetic, self-detachable, cancer cell spheroid model which provides the confined space of tumor microenvironment, convenient spheroid retrieval, immunostaining, treatment, and imaging. We formed void space within alginate macrobeads by ionic disintegration at a specific region inside. The macrobeads were further destabilized with bovine serum albumin to retrieve the spheroid cultured within void space. Quantitative analysis of the immunofluorescence images of the cultured spheroids showed enhanced expressions of the hypoxia-inducible factor-1α (HIF-1α) and carbonic anhydrase-9 (CA-9), like monolayer cultures of cancer cells in hypoxic conditions (0.2% oxygen). Furthermore, adding $CoCl_2$ to the cell culture media induces even higher amounts of HIF-

1α and CA-9 in the cultured spheroids. In conclusion, the present work highlighted the in-vitro spheroid model, which is closer to the tumor microenvironment and has user-friendly cell seeding, spheroid retrieval, and immunostaining steps.

Introduction

Abnormal tumor structure with insufficient blood, nutrient, and oxygen supply leads to the onset of hypoxia[1,2] and significant changes in cell characteristics.[1,2] For example, hypoxia induces epithelial-to-mesenchymal transition (EMT) of the cancer cells and alters protein synthesis, energy production, mitochondrial respiration, and lipid and carbon metabolism.[3] The resultant cells display "stem cell-like" properties[4] with increased expressions of several membrane protein markers, such as hypoxia-inducible factor-1α (HIF-1α) and carbonic anhydrase-9 (CA-9).[5–7]

Spheroids are widely used multicellular 3D models to mimic tumor microenvironments.[8,9] Spheroids develop nutrient, oxygen, and metabolic gradients leading to a heterogenous cell population with superior cell-to-cell and cell-to-extracellular matrix (ECM) interactions.[10–12] Three-dimensional cultures of cancer cells played a crucial role in anticancer drug screening and understanding tumor cell behavior.[13–15] Cancer cell spheroids usually form due to a lack of adhesion with the surface and subsequent aggregation. However, techniques based on this method need specialized training, resulting in a lack of reproducible results. In addition, the formed spheroids pose challenges in immunostaining, imaging, retrieval, and storage.[16,17]

Sodium alginate has been used as biocompatible polymer material to support cell growth in 3D scaffolds.[18,19] Alginate scaffolds have demonstrated several advantages for 3D cell culture, including their ability to support cell growth and function and mimic many tissues' extracellular matrix (ECM).[19,20] The porous structure of alginate scaffolds allows the exchange of nutrients and

waste products between cells and the surrounding environment. The biodegradability of the scaffold contributes to its eventual breakdown and removal. Further, alginate hydrogels formulated with different pore sizes showed diffusion of oxygen and other nutrients through the scaffold.[21,22]

Herein, we present a self-detachable model in a confined space for cancer cell spheroid formation to mimic the tumor microenvironment along with easy spheroid retrieval, immunostaining, treatment, and imaging. We prepared spheroids from the triple-negative breast cancer cells MDA-MB-231 and the pancreatic ductal adenocarcinoma cells BxPC-3. The cells were encaged within the void space of sodium alginate macrobeads to restrict the diffusion of oxygen and other nutrients. The interface between the macrobeads and void space was imaged and quantitated with a line profile. Each alginate bead contained one spheroid. Further, the beads were treated with bovine serum albumin (BSA) to destabilize sodium alginate and detach the formed spheroids. HIF-1α and CA-9 expressions were determined by immunofluorescence imaging and quantitative analysis to demonstrate hypoxic regions in the spheroids. The addition of cobalt (II) chloride in the cell culture medium further enhanced the expressions of the hypoxia markers in the spheroids.

Materials and Methods

Microbead preparation: Sodium alginate (0.7% w/v) was dissolved in MilliQ water (low conductivity ultra-pure water) and stirred for 4 hours. The resulting alginate gel was extruded dropwise into a solution of 7% (w/v) calcium chloride in MilliQ water using a syringe with a 28-gauge needle and curing for 5 minutes. Crosslinked calcium alginate microbeads were washed with MilliQ water.

Cell culture: The MDA-MB-231 and BxPC-3 cells were purchased from American Type Culture Collection (Manassas, VA) and cultured as recommended by the vendor. For normoxic conditions,

the cells were grown in an incubator at 37 °C containing 5% carbon dioxide and 21% oxygen. For the hypoxic conditions, cells were incubated in a hypoxia chamber (Coy In Vivo Hypoxic Cabinet System) with 5% carbon dioxide and 0.2% oxygen at 37 °C. For chemical induction of hypoxia, cells were treated with 25 μM $CoCl_2$ dissolved in DMEM media for 72 hours in an incubator at 37 °C containing 5% carbon dioxide and 21% oxygen.

Microbead disintegration in PBS: Crosslinked calcium alginate microbeads were washed with MilliQ water and suspended in phosphate-buffered saline (PBS) (137 mM NaCl, 10 mM phosphate, 2.7 mM KCl; pH 7.4) for 30 minutes to allow a partial exchange of calcium and sodium ions. The resultant smaller beads were treated with PBS, and a time-lapse video was recorded using a Zeiss confocal microscope (LSM 900, Airyscan-2) for 4 hours.

***Development of void space within alginate macrobeads and characterization*:** Crosslinked calcium alginate microbeads were washed with MilliQ water and suspended in PBS (30 minutes) to exchange calcium and sodium ions. The resultant microbeads were washed with MilliQ water, coated with sodium alginate gel (3% w/v), and dropped into a 7% w/v aqueous calcium chloride solution. Those beads were allowed to cure in calcium chloride for 20 minutes and labeled as macrobeads. The macrobeads were incubated in DMEM media for 8 hours and analyzed for void space inside. We repeated the above steps without PBS treatment for beads without void space, so microbeads did not partially disintegrate to form void space within alginate macrobeads. Developed macrobeads with and without void space were imaged under a microscope. Images of the region of interface between void space and macrobead were captured. The quantitative line intensity profile was analyzed at the interface region between the void space and the macrobead. The quantitative line intensity profile analysis was conducted using the ImageJ software (NIH, version 1.53f51).[23] To further confirm, microbeads with void space within were treated with

fluorescein-labeled BSA and time-lapse video recorded using a confocal fluorescence microscope (LSM 900, Airyscan-2) for 2.5 hours and 12 hours for macrobeads without the void space.[24]

***Spheroid cancer cell culture at void space inside alginate macrobeads*:** MDA-MB-231 and BxPC-3 cell pallets obtained from 70% confluent T-75 flasks were resuspended into 400 µL 0.7% w/v sodium alginate in DMEM media. Cells suspension was diluted so that about 2×10^4 cells were seeded in each microbead. The resulting cell suspension was extruded into a 7% w/v calcium chloride solution using a syringe (28G needle) and cured for 5 minutes. Next, the crosslinked calcium alginate microbeads were washed with MilliQ water and suspended in PBS (30 minutes) to exchange calcium and sodium ions. Resultant microbeads were washed with MilliQ water, coated with sodium alginate gel (3% w/v), and dropped into an aqueous 7% w/v calcium chloride solution. The beads were allowed to cure in a calcium chloride solution for 20 minutes and considered alginate macrobeads. Subsequently, the beads were washed with MilliQ water and incubated in DMEM media for 72 hours to allow the encaged cells to form a spheroid within void space (Figure 1A).

***Spheroid cancer cell culture by hanging drop method**:* Briefly, MDA-MB-231 spheroids were obtained by pipetting MDA-MB-231 cell suspension of 5,000 cells in 40 µL growth medium/well) into a Perfecta 3D Hanging Drop Plate (3D Biomatrix HDP1096-8). Spheroids were retrieved in the collecting plate after 3 days and used for further live/dead staining. Those stained spheroids were imaged under a confocal fluorescence microscope (LSM 900, Airyscan-2 by Carl Zeiss).

***Detachment of the cultured cancer cell spheroids from alginate macrobeads*:** To isolate the cultured spheroids, the alginate macrobeads were treated with 5% w/v BSA solution in PBS for 12 hours in the incubator. The macrobeads were imaged before and after BSA treatment. The

cancer cell spheroid was within an alginate macrobead before BSA treatment; however, it detached and moved outside the bead after BSA treatment. Isolated spheroids were imaged using a portable camera. The isolated spheroids were used for further immunostaining and analysis.

***Characterization of spheroids cultured at void space within alginate macrobead*:** The spheroids developed within the void space of alginate macrobeads were stained with a live/dead cell staining kit. Stained spheroids were imaged under a confocal fluorescence microscope (LSM 900, Airyscan-2) with FITC and RFP filters. The live fraction of cells was calculated as the ratio of green fluorescence intensity (live cells) to red fluorescence intensity (dead cells) by using the NIH ImageJ Software.[25]

Immunostaining and fluorescence microscopy of hypoxia markers: Isolated fixed spheroids were stained with DAPI, FITC labeled CA-9, and AF-647 labeled HIF-1α antibodies. The spheroids were imaged using a confocal fluorescence microscope, and the images were analyzed in ZEN software (Version 3.4.91.00000, Carl Zeiss Microscopy) for intensity quantification.

***$CoCl_2$ treatment of cancer cells encaged within void space of alginate macrobeads*:** For the alginate encaged cells, $CoCl_2$ (25 μM) loaded alginate gel was used to form the macrobeads and incubated in DMEM media containing 25 μM added $CoCl_2$. To induce hypoxia in monolayer cultures, the MDA-MB-231 and BxPC-3 cells were treated with 25 μM $CoCl_2$ in DMEM media for 72 hours.

Statistical Analysis: The statistical analyses were conducted using OriginPro 2021b software (Northampton, MA). The nonparametric Mann-Whitney and paired t-test evaluated the significant statistical differences within the treatment groups.

Results

First, we prepared calcium alginate microbeads. Subsequently, we partly disintegrated them to create the void space and coated them with another layer of calcium alginate to form the macrobeads. The cancer cell spheroids grew within the void space of the microbeads encased in the macrobeads (Figure 1A).

***Microbead preparation and disintegration in PBS*:**

Alginate microbeads were prepared by crosslinking sodium alginate with Ca^{2+} ions. Microscopic images of microbeads showed spherical structures with an average diameter of 1.7 ± 0.1 mm (Supplementary Figure S1). These microbeads were further used as a base for void space formation within alginate macrobeads. To form void space within alginate macrobeads, the microbeads were exposed to PBS for partial structural disintegration (Figure 1A). The alginate microbeads underwent a 13% surface area reduction after 10 minutes in PBS. However, after one hour, the surface area increased (by 28%), and the beads disintegrated in 4 hours (Supplementary Video 1). The 3D surface plots showed microbead contraction after 10 minutes, subsequent dilation after 1 hour, and collapse after 4 hours in PBS (Figure 1B).

Characterization of void space within alginate macrobeads:

The interface between the macrobead and void space within was imaged with 20X brightfield microscopy. The line profiles across the interface between macrobead and the inside void space demonstrated a sharp transition at 58 μm; however, the line across the interface between the macrobead and microbead inside shows an elevated peak at 58 μm distance. The image of the

interface reveals a difference between microbead within macrobead and void space within macrobead (Figure 1C).

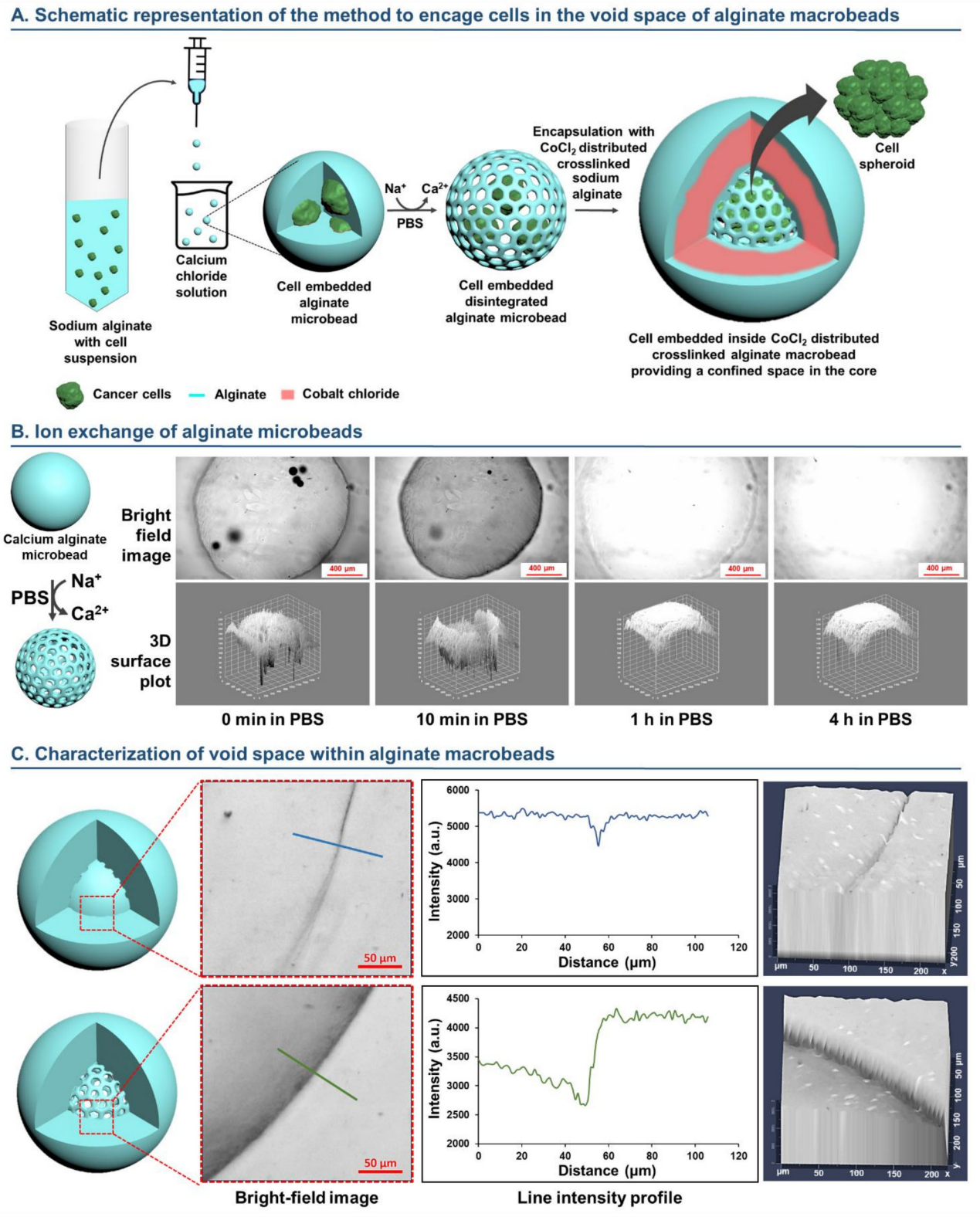

Figure 1: (A) Schematic representation of encaging cancer cells within void space of alginate macrobeads and subsequent spheroid formation. The green color depicts live cells in the spheroid

(see Figure 3C). **(B)** Left side schematics represent Na^+ and Ca^{2+} ion exchange of microbeads in PBS solution. The right-side top panel images show time-lapse brightfield images of an alginate microbead, and the bottom panel shows a 3D surface plot for the same images as a function of time in PBS. **(C)** The left side schematic represents alginate macrobeads with and without inside void space. The region showed on the schematics the interface between microbead and macrobead. The next panel shows a brightfield image of the same. Blue and green lines on the bright field image represent the line intensity profile across the microbead and macrobead interface and the interface region between void space and macrobead. The line intensity profile graph demonstrated altered intensity at the interface area. The right side shows brightfield images of the interface.

To further confirm the inside void spaces, a solution of fluorescein-labeled bovine serum albumin (BSA) was added to the macrobeads. Time-lapse fluorescence images were captured at the interface of macrobead and void space for 60 minutes. The diffusion pattern of fluorescein-labeled BSA was evaluated to determine the structure of the alginate macrobeads.[24] The images revealed BSA accumulation in the cavity within 15 minutes (Supplementary Video 2). However, the macrobeads without any void showed no accumulation of BSA in 60 minutes (Supplementary Video 3). The labeled BSA intensity profile plots show a gradual increase of green intensity in void space within macrobeads at 0, 15, 30, and 60 minutes; however, the microbead within microbead (i.e., no void space) shows constant low green intensity values up to 60 minutes (Figure 2).

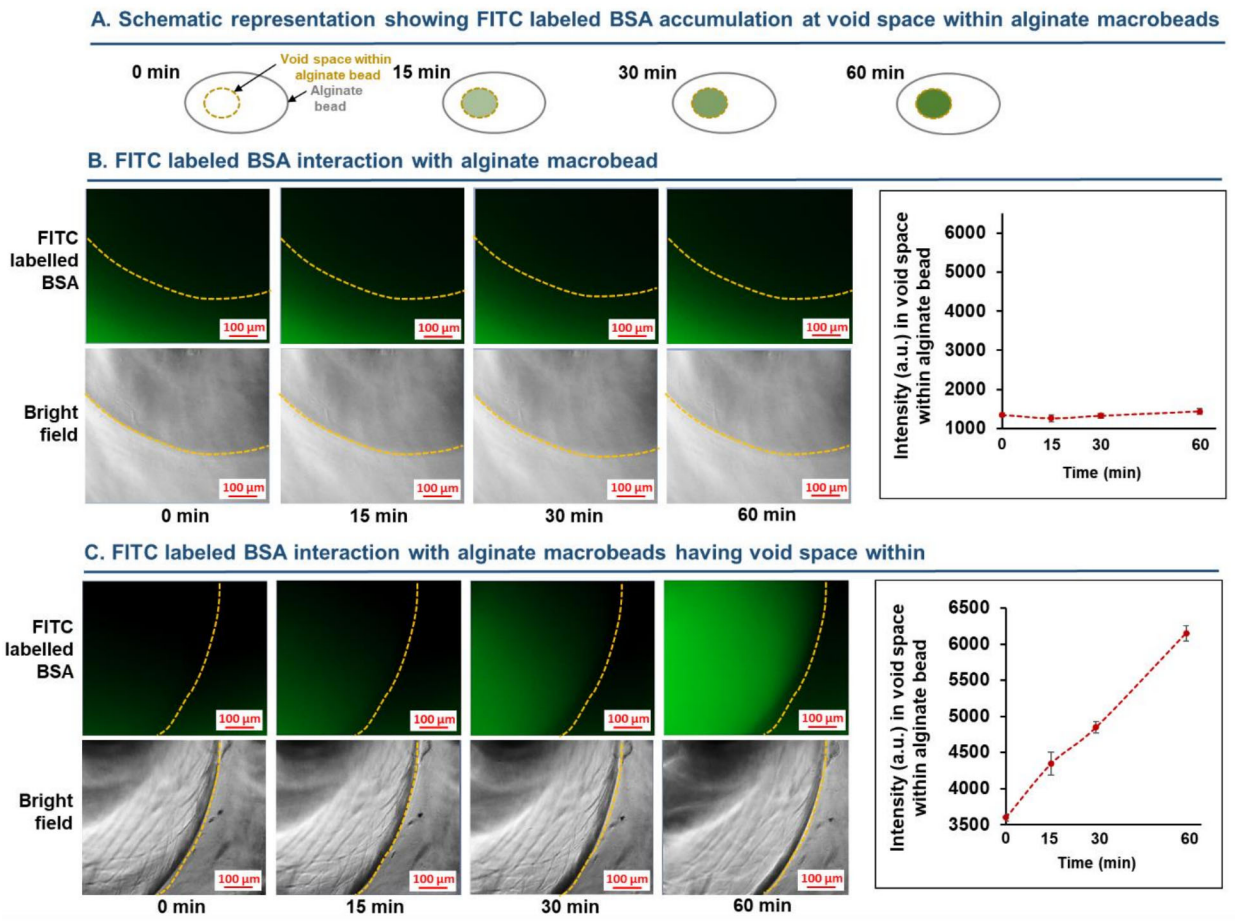

Figure 2: FITC labeled BSA was added to the alginate macrobeads with void spaces. The time-lapse video was recorded at the void space and macrobead interface region. (A) Schematic representation of time-dependent accumulation of FITC labeled BSA at the void space within alginate macrobeads. **(B)** Time-lapse images for up to 60 minutes showing FITC fluorescence and brightfield images of macrobead and microbead (without PBS treated) interface. The right-side graph represents time-dependent fluorescence intensity in microbeads inside macrobeads. Graph of intensity profile against the time of BSA incubation shows a gradual increase of green fluorescence intensity in void space within macrobead up to 60 minutes. **(C)** Time-lapse images for 60 minutes showing FITC and brightfield fluorescence images of macrobead and void space within (microbead with PBS treatment) interface. The right side graph represents the time-dependent fluorescence intensity of void space within the microbead and shows steady green intensity values up to 60 minutes (n = 5).

Characterization of spheroids obtained from void spaces inside the alginate macrobeads:

To demonstrate the generality of our approach, we grew spheroids from metastatic triple-negative breast cancer (MBA-MB-231) and pancreatic ductal adenocarcinoma (PANC1) cells. Optical

images of macrobeads with spheroid in the void space show a white mass inside. BSA-treated macrobeads show collapsed alginate microbeads detached from the intact spheroids. A bright field image revealed a 1.2 ± 0.1 mm spheroid inside the alginate macrobead of 5.8 ± 0.2 mm diameter (Figure 3A). Figure 3B shows a fluorescence microscopic image of a spheroid obtained from the hanging drop method and a spheroid obtained from void space within alginate macrobeads, stained using a commercially available live/dead cell staining kit (red: dead cells; green: live cells). The fraction of live cells was quantitated by measuring the ratio of green fluorescence intensity (live cells) to red fluorescence intensity (dead cells) of the spheroids (Figure 3B). Statistical analysis showed no significant difference in live cells in spheroids obtained from the hanging drop method and the void space within alginate macrobeads.[26]

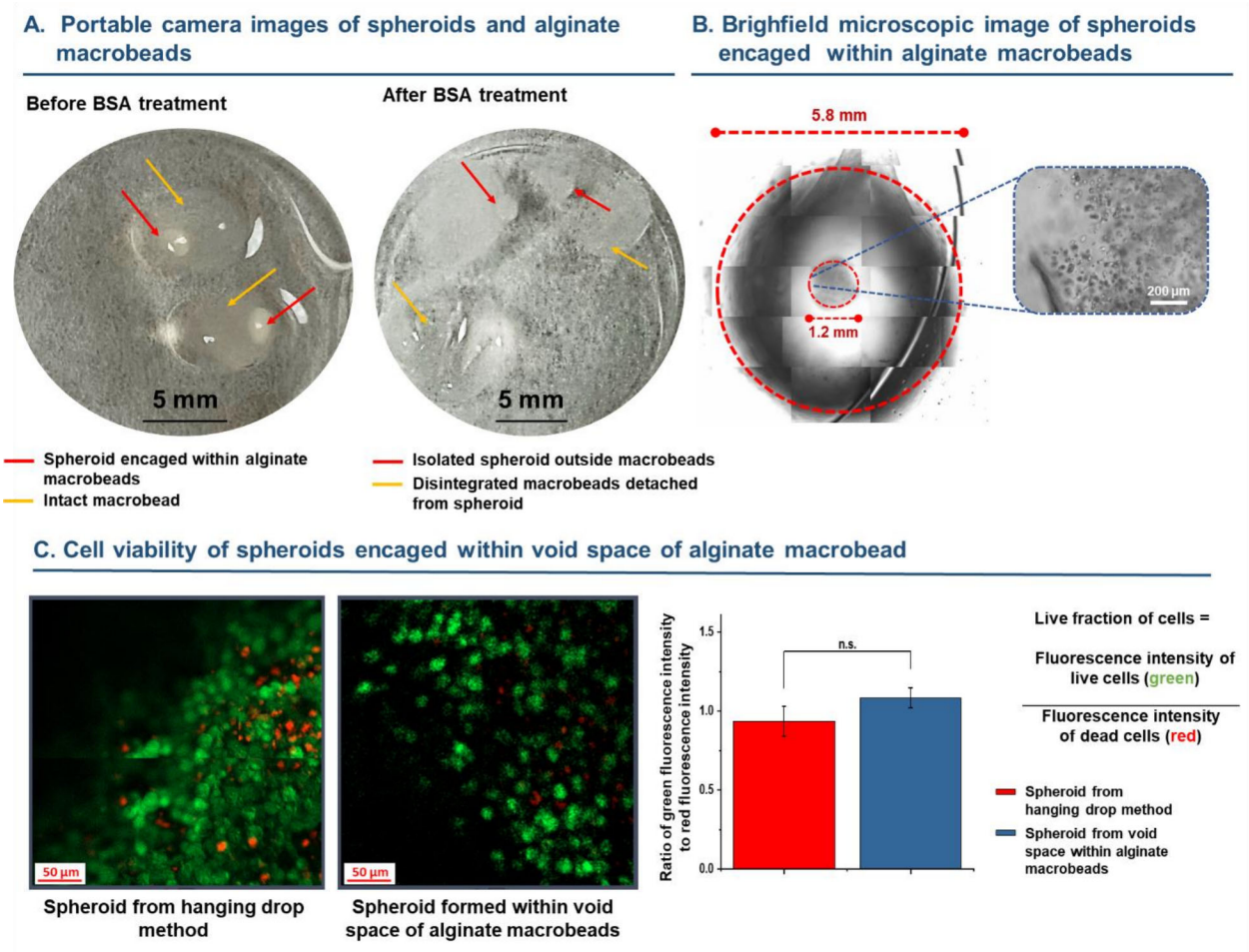

Figure 3: (A) Optical images of spheroids within alginate macrobeads and macrobeads with and without BSA treatment. The yellow arrows indicate intact macrobeads (left side image) and disintegrated macrobead (center image). The red arrow indicates a spheroid within the void space of an intact macrobead (left side image) and a spheroid isolated from a disintegrated macrobead (center image). **(B)** A bright field image of a spheroid within the void space of an alginate macrobead revealed a 1.2 ± 0.1 mm spheroid inside an alginate macrobead of 5.8 ± 0.2 mm diameter. **(C)** Confocal fluorescence microscopy image of MDA-MB-231 cell spheroid obtained from traditional hanging drop method and void space within alginate macrobeads, stained with a live/dead staining kit. Images show merged red and green channels representing live and dead cells. The graph compares the live fraction of cells in spheroid obtained within the void space of alginate macrobeads and from the hanging drop method. Data were analyzed using the paired t-test ($P > 0.05$, $n = 3$).

Carbonic anhydrase-9 (CA-9) expression variation in cancer cell spheroids from alginate microbeads, alginate macrobeads with void space, and $CoCl_2$ treated macrobeads:

The membrane-bound enzyme CA-9 regulates the pH of cancer cells, specifically for hypoxic tumors.[27] Upregulation of CA-9 is reported in various cancers, including breast, pancreatic, and renal malignancies, and is a tumor hypoxia marker.[28] To measure CA-9 expression of spheroids from triple-negative breast cancer (MDA-MB-231) and pancreatic cancer (BxPC-3) cells obtained by our method, the cultured spheroids were immunostained with FITC-labeled CA-9 antibody and imaged by confocal fluorescence microscopy (green: CA-9; blue: cell nuclei). MDA-MB-231 and BxPC-3 cell spheroids exhibited enhanced CA-9 expression in hypoxia and in the presence of $CoCl_2$ compared to normoxia (i.e., spheroids in alginate microbeads). Quantitative image analysis revealed significant differences between spheroids from alginate encapsulation, void space within alginate macrobeads, and void space within $CoCl_2$-treated alginate macrobeads. Specifically, in spheroids obtained from void space within alginate macrobeads, CA-9 expression was higher by approximately 2-fold for MDA-MB-231 and BxPC-3 cell spheroids compared to normoxia. Furthermore, for spheroids from void space within $CoCl_2$-treated alginate macrobeads, the CA-9 expression was highest, with an increase of approximately 4-fold for both MDA-MB-231 and BxPC-3 cell spheroids (Figure 4).

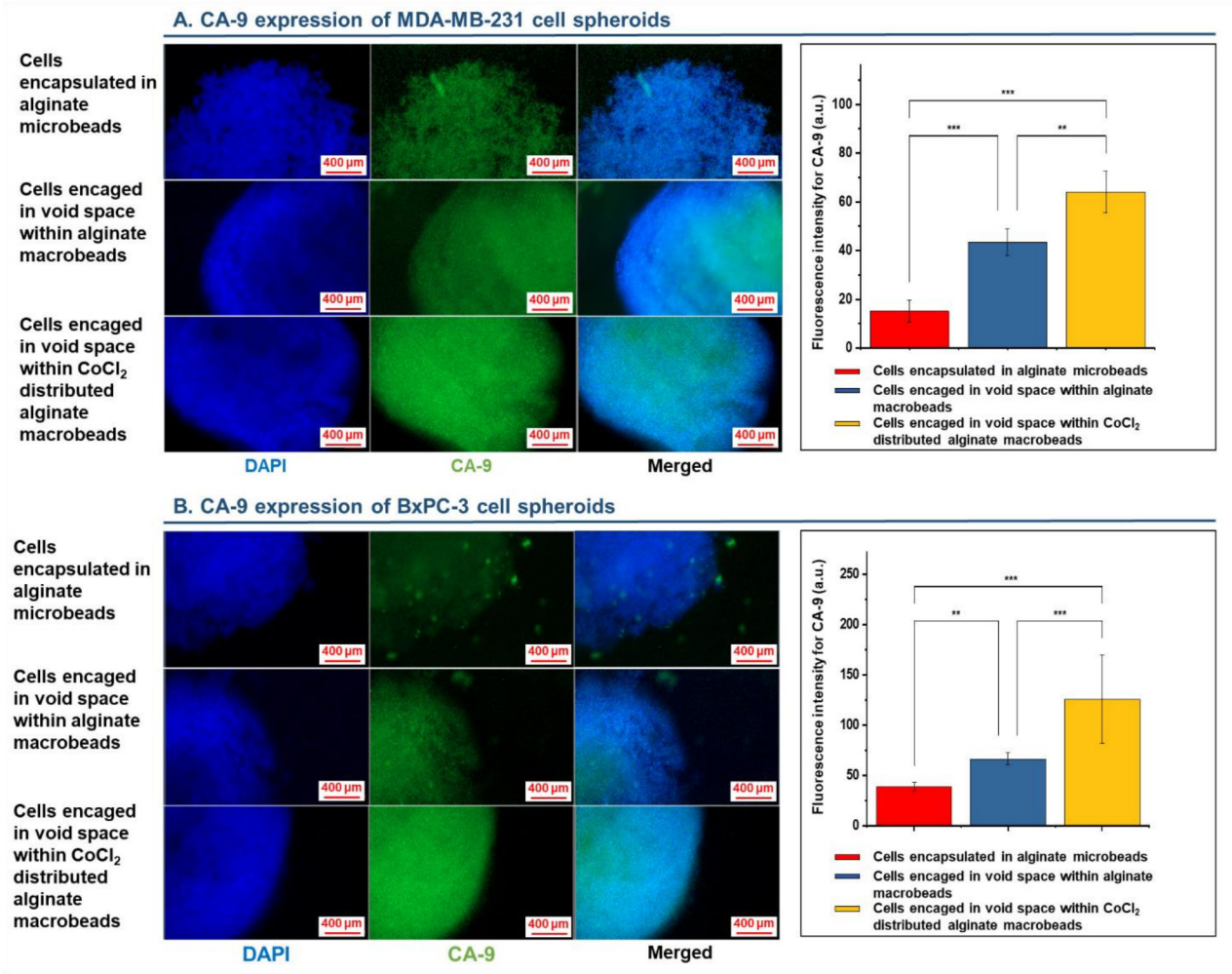

Figure 4: Representative fluorescence microscopic images of **(A)** MDA-MB-231 and **(B)** BxPC-3 cell spheroids obtained from alginate microbeads and alginate macrobeads with void space without and with $CoCl_2$. Blue and green channels represent DAPI and FITC-labeled CA-9 antibody-stained spheroids. The side graphs show the intensity for CA-9 in spheroids obtained from either cell encapsulated in alginate microbeads or encaged in void space within alginate macrobeads or encaged in void space within $CoCl_2$ treated alginate macrobeads. Data were analyzed using the nonparametric Mann-Whitney test, ***P < 0.01, **P < 0.05, n = 3.

HIF-1α expression variation in cancer cell spheroids from alginate microbeads, alginate macrobeads with void space, and $CoCl_2$-treated macrobeads:

HIF-1α is critical in cellular adaptation to hypoxia and promotes tumor growth, survival, and metastasis. HIF-1α is considered a crucial marker for hypoxic tumor regions.[29] Therefore, spheroids obtained under different culture conditions were analyzed for HIF-1α expression. MDA-MB-231 and BxPC-3 cell spheroids obtained from alginate microbeads, alginate macrobeads with void space, with and without $CoCl_2$ were immunostained with Alexa Fluor 647 (AF-647) labeled anti-HIF-1α antibody and imaged employing confocal fluorescence microscopy (Figure 5). In the images, the purple color shows HIF-1α expression, and blue represents the nuclei of the cells. The images indicate enhanced HIF-1α expression under hypoxia and in the presence of $CoCl_2$ compared to normoxia (i.e., spheroids in microbeads) for both MDA-MB-231 and BxPC-3 cell spheroids. Quantitative fluorescence intensity analysis demonstrated significant differences between spheroids from alginate microbeads (normoxia) and alginate macrobeads with void space with and without $CoCl_2$. In spheroid obtained from void space within alginate macrobeads, the HIF-1α expression was higher by 2 and 4 folds in MDA-MB-231 and BxPC-3 cells, respectively, compared to normoxia. In spheroid from void space within $CoCl_2$ alginate macrobeads, the HIF-1α expression was highest, 3 and 7-fold more in MDA-MB-231 and BxPC-3 cells, respectively, compared to normoxia (Figure 5).

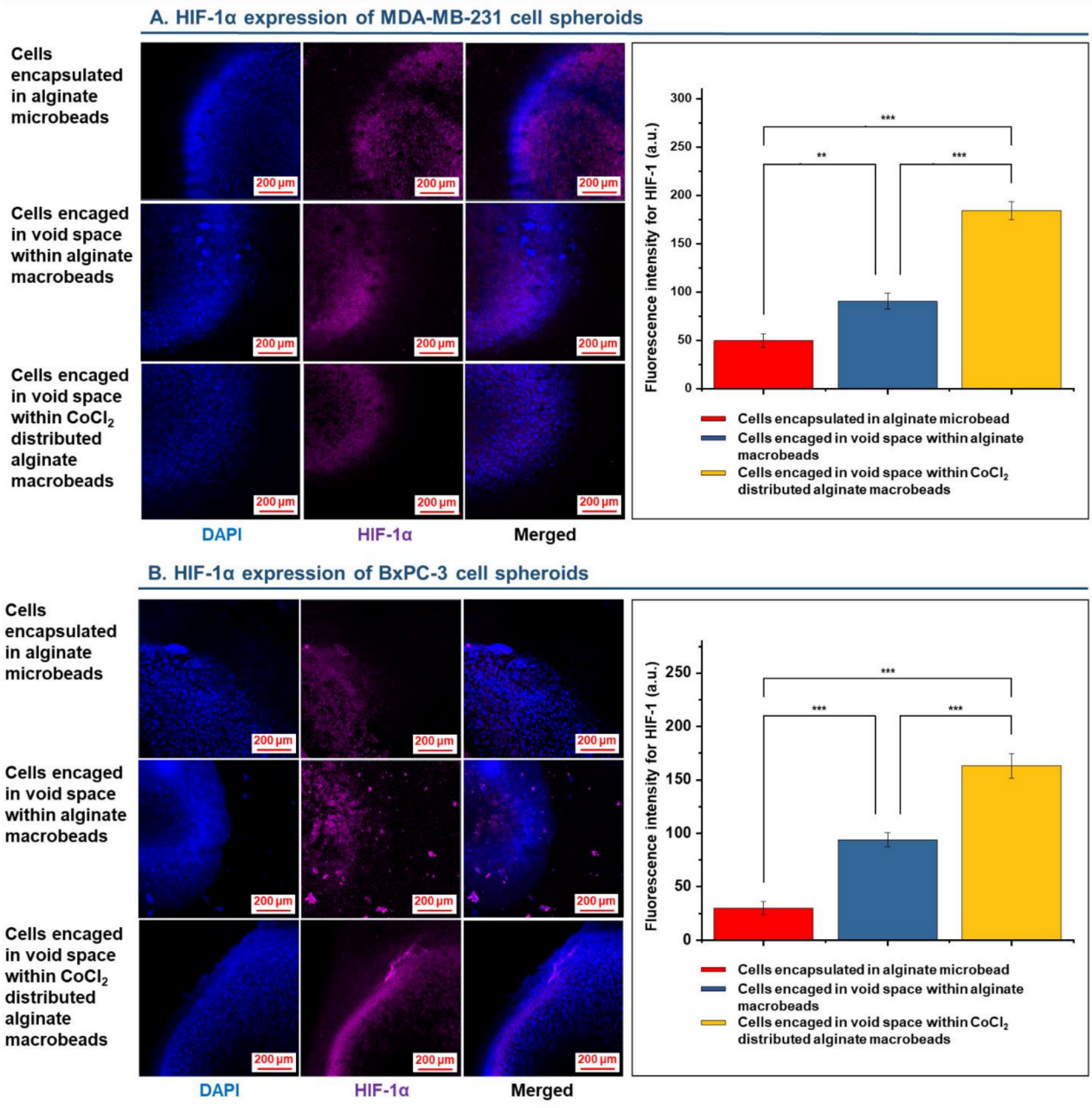

Figure 5: Representative fluorescence microscopic images of **(A)** MDA-MB-231 and **(B)** BxPC-3 cell spheroids obtained from alginate microbeads (normoxia), alginate macrobeads with voids, and alginate macrobeads with void and in the presence of $CoCl_2$. Blue and green colors represent DAPI and HIF-1α, respectively. The graph shows the intensity of the purple color (HIF-1α) in the spheroids. Data were analyzed using the nonparametric Mann-Whitney test, ***$P < 0.01$, **$P < 0.05$, $n = 3$.

CA-9 expression on MDA-MB-231 and BxPC-3 cells isolated from spheroids cultured in different conditions:

MDA-MB-231 and BxPC-3 cells were isolated from the cultured spheroids obtained from alginate microbeads and alginate macrobeads with void space with and without $CoCl_2$. Subsequently, the cells were resuspended in PBS and immunostaining with FITC labeled CA-9 antibody. The fluorescence microscopic images (Figure 6) indicate enhanced CA-9 expressions (green) in MDA-MB-231 and BxPC-3 cells isolated from spheroids cultured in the void space within alginate macrobeads and void space within $CoCl_2$ containing alginate macrobeads compared to spheroids obtained from alginate microbeads. Quantitative fluorescence intensity analysis of CA-9 expressions demonstrated a significant difference between cells isolated from spheroids obtained from alginate microbeads, void space within alginate macrobeads, and void space within $CoCl_2$-treated alginate macrobeads. In cells of spheroid obtained from void space within alginate macrobeads, the CA-9 expression was higher by 1.5-fold and 2-fold in MDA-MB-231 and BxPC-3 cells, respectively, compared to normoxia. In cells of spheroids obtained from void space within $CoCl_2$-treated alginate macrobeads, the CA-9 expression was highest (enhanced by 2-fold and 3-fold in MDA-MB-231 and BxPC-3 cells, respectively, compared to normoxia; Figure 6).

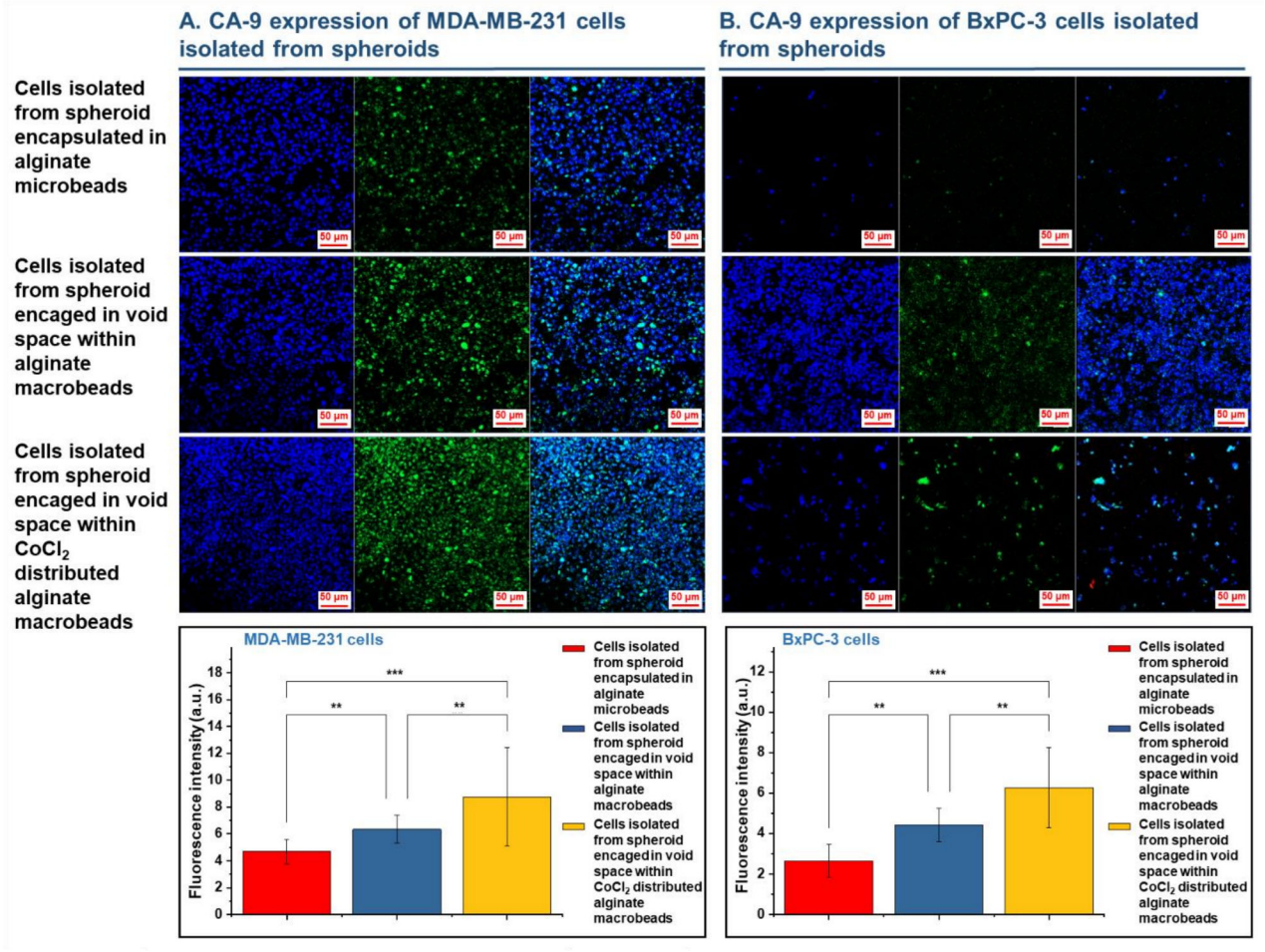

Figure 6. Representative fluorescence microscopic images indicating CA-9 (green) expression and nuclei (blue) in monolayer cultures of MDA-MB-231 **(A)** and BxPC-3 cells **(B)** isolated from MDA-MB-231 and BxPC-3 cell spheroids grown in normoxic, hypoxic, and $CoCl_2$ exposed conditions. The bottom graph represents fluorescence intensity for the CA-9 filter at normoxic, hypoxic, and $CoCl_2$ exposed conditions. Data were analyzed using the nonparametric Mann-Whitney test, ***P < 0.01, **P < 0.05, n = 3.

CA-9 and HIF-1α expressions on monolayer cultures of MDA-MB-231 and BxPC-3 cells in normoxic, hypoxic, and $CoCl_2$ treated conditions:

To validate increased CA-9 and HIF-1α expressions in monolayer cultures of cells obtained from the spheroids, the MDA-MB-231 and BxPC-3 cells were cultured as monolayers in normoxia, hypoxia, and normoxia with $CoCl_2$ containing media for 72 hours. Subsequently, we evaluated CA-9 and HIF-1α expressions by immunofluorescence imaging (Figure 7; green: CA-9, red: HIF-

1α, and blue: cell nuclei). Optical microscopy revelated that the cells were healthy in the presence of 25 μM $CoCl_2$ in the culture media (DMEM). However, a higher concentration of $CoCl_2$ (50 μM) caused altered cell morphology and cytotoxicity (Supplementary Figure S2). Quantitative fluorescence intensity analysis of CA-9 and HIF-1α expressions demonstrated a significant difference between normoxic, hypoxic, and $CoCl_2$ exposed conditions. In hypoxia, the CA-9 and HIF-1α expressions were higher by 2-fold in both MDA-MB-231 and BxPC-3 cells, respectively, compared to normoxia. In the presence of added $CoCl_2$, the CA-9 and HIF-1α expressions were the highest, 4-fold increase in both MDA-MB-231 and BxPC-3 cells, respectively, compared to normoxia (Figure 7).

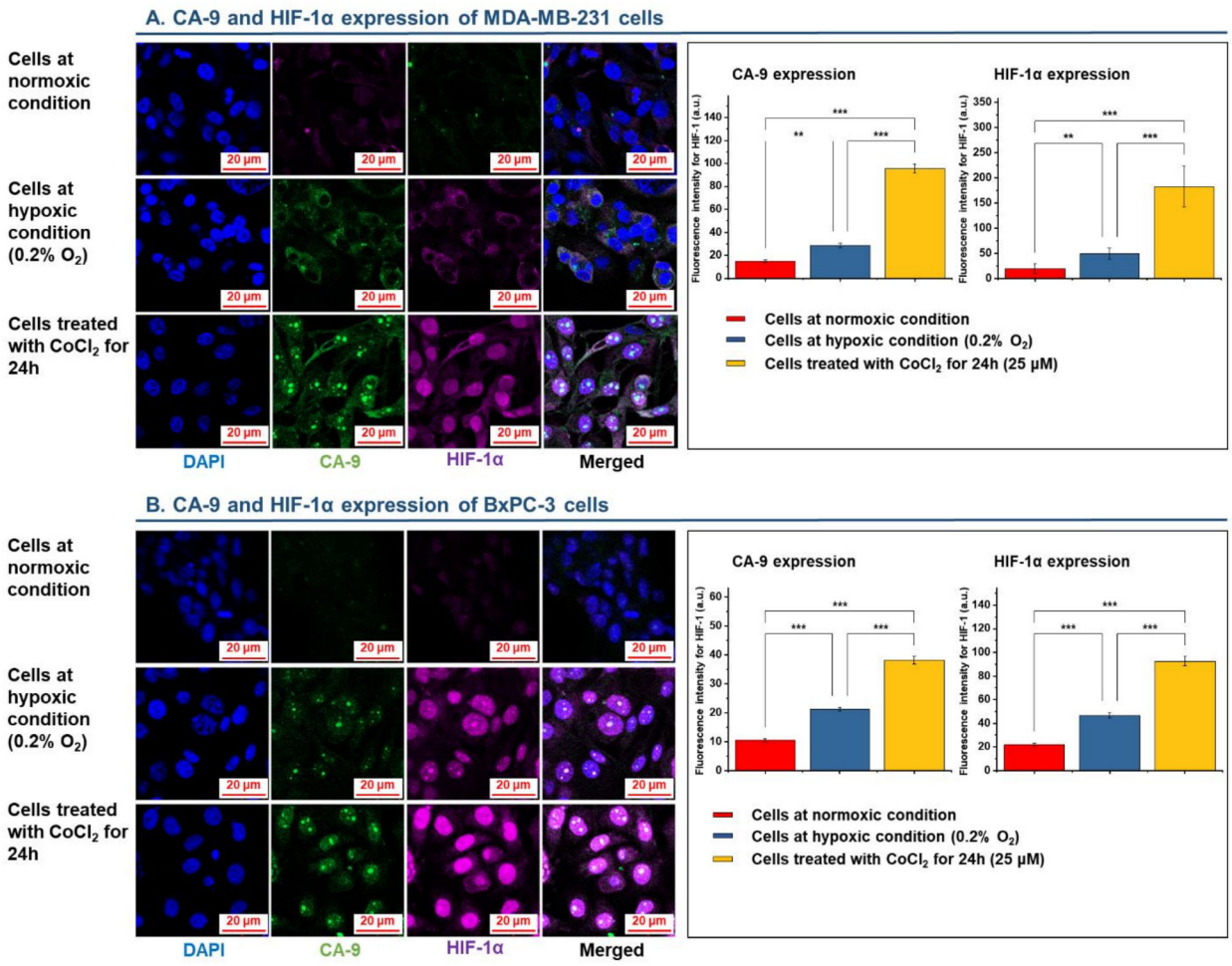

Figure 7: Representative fluorescence microscopic images indicating CA-9 (green) and HIF-1α (purple) expressions and nuclei (blue) of MDA-MB-231 cells **(A)** and BxPC-3 cells **(B)** at normoxic, hypoxic, and $CoCl_2$ exposed conditions. The right side graph represents image intensity for CA-9 and HIF-1α at normoxic, hypoxic, and $CoCl_2$ exposed conditions. Data were analyzed using the nonparametric Mann-Whitney test, ***P < 0.01, **P < 0.05, n = 10.

Discussions

Microbeads (1.7 ± 0.1 mm) and macrobeads (5.8 ± 0.2 mm) were formed by crosslinking sodium alginate with calcium ions. A higher sodium alginate concentration (3% w/v) was used to create the macrobeads compared to the microbeads (0.7% w/v). Calcium ion crosslinked microbeads from 0.7% (w/v) sodium alginate disintegrate in phosphate-buffered saline (PBS) due to the exchange between the calcium ions in the beads and the sodium ions in the PBS. In addition,

calcium and sodium ion exchange compromised the three-dimensional structure of the microbeads.[30,31] The bright field images and the 3D surface plots of the microbeads showed the bead surface more susceptible to disintegration and the overall shape of the disintegrated beads (Figure 1B). As the weakened microbeads disintegrate within the macrobeads, the resulting void spaces serve as scaffolds for the spheroid culture of the cancer cells. The line profile across the interface between the alginate macrobead and void space demonstrated a sharp peak in the line intensity profile, possibly due to the differences in density and refractive index of the alginate macrobead and the void space (Figure 1C).

The void spaces provide the environment for the cancer cells' three-dimensional growth, enabling spheroids' formation. When a solution of FITC-labeled BSA was added to the macrobeads, the protein molecules diffused through the alginate matrix and accumulated within the void spaces. Photographic images demonstrated spheroid growth inside the void spaces of the alginate macrobeads (Figure 2A). A higher concentration of BSA disrupted the alginate matrix and detached the growing spheroids (Figure 2A).[32,33] Possibly, BSA alters alginate chain entanglements, making the macrobeads structurally weak and facilitating spheroid.[34] A bright field image of a spheroid within the void space of an alginate macrobead revealed intact spheroid organization (Figure 2B). Live and dead cell staining showed that 95% of cancer cells are viable in the spheroid within the void space of an alginate macrobead compared to 92% of viable cells in the spheroids obtained by the hanging drop method (Figure 2C).

To validate the formation of hypoxic niches in the cultured cancer cell spheroids, we determined the presence of two hypoxia marker proteins, carbonic anhydrase-9 (CA-9) and hypoxia-inducible factor-1α (HIF-1α). CA-9 expression is regulated by the amount of oxygen and is a transmembrane protein biomarker for tumor hypoxia.[35] Similarly, HIF-1α, a transcription factor,

plays a critical role in the cellular responses to hypoxia.[36] Higher expressions of CA-9 and HIF-1α correlate with poor prognosis of many solid tumors, including TNBC and pancreatic cancer.[37] Our alginate microbeads (1.7 ± 0.1 mm diameter) provide an oxygenated environment for spheroid formation and growth, as the small size allows rapid diffusion of oxygen and nutrients. Consequently, CA-9 and HIF-1α expression levels in the cancer cell spheroids obtained from alginate microbeads are relatively low compared to spheroids from the void space within alginate macrobeads (Figures 4 and 5). However, for the larger macrobeads (5.8 ± 0.2 mm diameter), the oxygen diffusion into the void space is limited by the surrounding alginate layer and the density of cancer cells, leading to the development of hypoxic regions and higher CA-9 and HIF-1α expressions in the spheroids. $CoCl_2$ induces the expression of HIF-1α on cancer cells which upregulates CA-9.[38] Hence, the spheroids obtained from $CoCl_2$-containing alginate macrobeads exhibit the highest levels of CA-9 (Figure 4) and HIF-1α (Figure 5) expressions, similar to the monolayer cultures of the cancer cells in the presence of $CoCl_2$ (Figure 7).

Conclusions

We present a new strategy to prepare cancer cell spheroids based on void spaces inside crosslinked calcium alginate hydrogel beads. We observed that limited diffusion of air and nutrients led to hypoxic niches in the cultured cancer cell spheroids. The addition of $CoCl_2$ further enhances hypoxia development. The presented in-vitro spheroid model is closer to the tumor microenvironment and has easy cell seeding, spheroid retrieval, and immunostaining steps with uniform 1.2 mm cell spheroids. The alginate hydrogel macrobeads have the potential to facilitate the testing of new anticancer drugs and delivery systems, primarily directed to the hypoxic regions.

Moreover, this in-vitro spheroid model of void space within alginate macrobead can be an effective preclinical model of 3D patient-derived cell spheroids with considerable translational potential.

ASSOCIATED CONTENT

Supporting Information

Additional experimental data included in supplementary information such as calcium ions of alginate exchange with sodium ions in the presence of phosphate buffer saline (PBS) solution (Supplementary Video 1), FITC labeled BSA accumulation at void space within alginate macrobeads (Supplementary Video 2), FITC labeled BSA interaction with alginate macrobeads having alginate microbead inside (Supplementary Video 3), Brightfield microscopic images of alginate microbeads captured under 4X magnification (Supplementary Figure S1), Brightfield microscopic images of MDA-MB-231 and BxPC-3 cells treated with 25 μM and 50 μM $CoCl_2$ (Supplementary Figure S2).

AUTHOR INFORMATION

Corresponding Author

* Sanku.Mallik@ndsu.edu

Author Contributions

The manuscript was written through the contributions of all authors. All authors have approved the final version of the manuscript.

Funding Sources

The NIH grant 2 R01GM 114080, NSF EPSCoR Track-1 Cooperative Agreement OIA #1946202, and DaCCoTA Center award (NIGMS U54 GM128729) supported this study. Any opinions,

findings, conclusions, or recommendations expressed in this material are those of the author(s) and do not necessarily reflect the views of the NSF.

Acknowledgement

We would acknowledge the Core Confocal Microscopy Facility, Department of Pharmaceutical Sciences, North Dakota State University, supported by the DaCCoTa CTR award U54GM128729.

REFERENCES

(1) Hompland, T.; Fjeldbo, C. S.; Lyng, H. Tumor Hypoxia as a Barrier in Cancer Therapy: Why Levels Matter. *Cancers (Basel).* **2021**, *13* (3), 499.

(2) Shibuya, K.; Saito, H.; Nishikido, F.; Takahashi, M.; Yamaya, T. Oxygen Sensing Ability of Positronium Atom for Tumor Hypoxia Imaging. *Commun. Phys.* **2020**, *3* (1), 173.

(3) Eales, K. L.; Hollinshead, K. E. R.; Tennant, D. A. Hypoxia and Metabolic Adaptation of Cancer Cells. *Oncogenesis* **2016**, *5* (1), e190–e190.

(4) Cui, X. Y.; Skretting, G.; Jing, Y.; Sun, H.; Sandset, P. M.; Sun, L. Hypoxia Influences Stem Cell-like Properties in Multidrug Resistant K562 Leukemic Cells. *Blood Cells, Mol. Dis.* **2013**, *51* (3), 177–184.

(5) Lequeux, A.; Noman, M. Z.; Xiao, M.; Van Moer, K.; Hasmim, M.; Benoit, A.; Bosseler, M.; Viry, E.; Arakelian, T.; Berchem, G.; Chouaib, S.; Janji, B. Targeting HIF-1 Alpha Transcriptional Activity Drives Cytotoxic Immune Effector Cells into Melanoma and Improves Combination Immunotherapy. *Oncogene* **2021**, *40* (28), 4725–4735.

(6) McDonald, P. C.; Chafe, S. C.; Brown, W. S.; Saberi, S.; Swayampakula, M.; Venkateswaran, G.; Nemirovsky, O.; Gillespie, J. A.; Karasinska, J. M.; Kalloger, S. E.; Supuran, C. T.; Schaeffer, D. F.; Bashashati, A.; Shah, S. P.; Topham, J. T.; Yapp, D. T.; Li, J.; Renouf, D. J.; Stanger, B. Z.; Dedhar, S. Regulation of PH by Carbonic Anhydrase 9 Mediates Survival of Pancreatic Cancer Cells With Activated KRAS in Response to

Hypoxia. *Gastroenterology* **2019**, *157* (3), 823–837.

(7) Codony, V. L.; Tavassoli, M. Hypoxia-Induced Therapy Resistance: Available Hypoxia-Targeting Strategies and Current Advances in Head and Neck Cancer. *Transl. Oncol.* **2021**, *14* (3), 101017.

(8) Wang, T.; Wang, L.; Wang, G.; Zhuang, Y. Leveraging and Manufacturing in Vitro Multicellular Spheroid-Based Tumor Cell Model as a Preclinical Tool for Translating Dysregulated Tumor Metabolism into Clinical Targets and Biomarkers. *Bioresour. Bioprocess.* **2020**, *7*, 1–34.

(9) Thakuri, P. S.; Liu, C.; Luker, G. D.; Tavana, H. Biomaterials-Based Approaches to Tumor Spheroid and Organoid Modeling. *Adv. Healthc. Mater.* **2018**, *7* (6), 1700980.

(10) Audoin, M.; Søgaard, M. T.; Jauffred, L. Tumor Spheroids Accelerate Persistently Invading Cancer Cells. *Sci. Rep.* **2022**, *12* (1), 14713.

(11) Lim, W.; Park, S. A Microfluidic Spheroid Culture Device with a Concentration Gradient Generator for High-Throughput Screening of Drug Efficacy. *Molecules*. 2018.

(12) Weltin, A.; Hammer, S.; Noor, F.; Kaminski, Y.; Kieninger, J.; Urban, G. A. Accessing 3D Microtissue Metabolism: Lactate and Oxygen Monitoring in Hepatocyte Spheroids. *Biosens. Bioelectron.* **2017**, *87*, 941–948.

(13) Kanebratt, K. P.; Janefeldt, A.; Vilén, L.; Vildhede, A.; Samuelsson, K.; Milton, L.; Björkbom, A.; Persson, M.; Leandersson, C.; Andersson, T. B.; Hilgendorf, C. Primary Human Hepatocyte Spheroid Model as a 3D In Vitro Platform for Metabolism Studies. *J. Pharm. Sci.* **2021**, *110* (1), 422–431.

(14) Zanoni, M.; Piccinini, F.; Arienti, C.; Zamagni, A.; Santi, S.; Polico, R.; Bevilacqua, A.; Tesei, A. 3D Tumor Spheroid Models for in Vitro Therapeutic Screening: A Systematic Approach to Enhance the Biological Relevance of Data Obtained. *Sci. Rep.* **2016**, *6* (1), 19103.

(15) Lu, H.; Stenzel, M. H. Multicellular Tumor Spheroids (MCTS) as a 3D in Vitro Evaluation

Tool of Nanoparticles. *Small* **2018**, *14* (13), 1702858.

(16) Griffin, K. H.; Fok, S. W.; Kent Leach, J. Strategies to Capitalize on Cell Spheroid Therapeutic Potential for Tissue Repair and Disease Modeling. *npj Regen. Med.* **2022**, *7* (1), 70.

(17) Han, S. J.; Kwon, S.; Kim, K. S. Challenges of Applying Multicellular Tumor Spheroids in Preclinical Phase. *Cancer Cell Int.* **2021**, *21*, 1–19.

(18) Wu, Z.; Li, Q.; Xie, S.; Shan, X.; Cai, Z. In Vitro and in Vivo Biocompatibility Evaluation of a 3D Bioprinted Gelatin-Sodium Alginate/Rat Schwann-Cell Scaffold. *Mater. Sci. Eng. C* **2020**, *109*, 110530.

(19) Martău, G. A.; Mihai, M.; Vodnar, D. C. The Use of Chitosan, Alginate, and Pectin in the Biomedical and Food Sector—Biocompatibility, Bioadhesiveness, and Biodegradability. *Polymers (Basel).* **2019**, *11* (11), 1837.

(20) Enck, K.; Tamburrini, R.; Deborah, C.; Gazia, C.; Jost, A.; Khalil, F.; Alwan, A.; Orlando, G.; Opara, E. C. Effect of Alginate Matrix Engineered to Mimic the Pancreatic Microenvironment on Encapsulated Islet Function. *Biotechnol. Bioeng.* **2021**, *118* (3), 1177–1185.

(21) Kang, S.-M.; Lee, J.-H.; Huh, Y. S.; Takayama, S. Alginate Microencapsulation for Three-Dimensional in Vitro Cell Culture. *ACS Biomater. Sci. Eng.* **2020**, *7* (7), 2864–2879.

(22) Chaicharoenaudomrung, N.; Kunhorm, P.; Promjantuek, W.; Heebkaew, N.; Rujanapun, N.; Noisa, P. Fabrication of 3D Calcium-alginate Scaffolds for Human Glioblastoma Modeling and Anticancer Drug Response Evaluation. *J. Cell. Physiol.* **2019**, *234* (11), 20085–20097.

(23) Kale, N.; Nandi, S.; Patil, A.; Patil, Y.; Banerjee, S.; Khandare, J. Nanocarrier Anticancer Drug-Conjugates Cause Higher Cellular Deformations: Culpable for Mischief. *Biomater. Sci.* **2020**, *8* (20), 5729–5738.

(24) Hu, M.; Zheng, G.; Zhao, D.; Yu, W. Characterization of the Structure and Diffusion

Behavior of Calcium Alginate Gel Beads. *J. Appl. Polym. Sci.* **2020**, *137* (31), 48923.

(25) Kwapiszewska, K.; Michalczuk, A.; Rybka, M.; Kwapiszewski, R.; Brzózka, Z. A Microfluidic-Based Platform for Tumour Spheroid Culture, Monitoring and Drug Screening. *Lab Chip* **2014**, *14* (12), 2096–2104.

(26) Nzou, G.; Wicks, R. T.; Wicks, E. E.; Seale, S. A.; Sane, C. H.; Chen, A.; Murphy, S. V; Jackson, J. D.; Atala, A. J. Human Cortex Spheroid with a Functional Blood Brain Barrier for High-Throughput Neurotoxicity Screening and Disease Modeling. *Sci. Rep.* **2018**, *8* (1), 7413.

(27) Sedlakova, O.; Svastova, E.; Takacova, M.; Kopacek, J.; Pastorek, J.; Pastorekova, S. Carbonic Anhydrase IX, a Hypoxia-Induced Catalytic Component of the PH Regulating Machinery in Tumors. *Front. Physiol.* **2014**, *4*, 400.

(28) Pastorekova, S.; Gillies, R. J. The Role of Carbonic Anhydrase IX in Cancer Development: Links to Hypoxia, Acidosis, and Beyond. *Cancer Metastasis Rev.* **2019**, *38*, 65–77.

(29) Infantino, V.; Santarsiero, A.; Convertini, P.; Todisco, S.; Iacobazzi, V. Cancer Cell Metabolism in Hypoxia: Role of HIF-1 as Key Regulator and Therapeutic Target. *Int. J. Mol. Sci.* **2021**, *22* (11), 5703.

(30) Lee, K. Y.; Mooney, D. J. Alginate: Properties and Biomedical Applications. *Prog. Polym. Sci.* **2012**, *37* (1), 106–126.

(31) Urbanova, M.; Pavelkova, M.; Czernek, J.; Kubova, K.; Vyslouzil, J.; Pechova, A.; Molinkova, D.; Vyslouzil, J.; Vetchy, D.; Brus, J. Interaction Pathways and Structure–Chemical Transformations of Alginate Gels in Physiological Environments. *Biomacromolecules* **2019**, *20* (11), 4158–4170.

(32) Chaturvedi, K.; Ganguly, K.; More, U. A.; Reddy, K. R.; Dugge, T.; Naik, B.; Aminabhavi, T. M.; Noolvi, M. N. Sodium Alginate in Drug Delivery and Biomedical Areas. In *Natural polysaccharides in drug delivery and biomedical applications*; Elsevier, 2019; pp 59–100.

(33) Sarıyer, S.; Duranoğlu, D.; Doğan, Ö.; Küçük, İ. PH-Responsive Double Network

Alginate/Kappa-Carrageenan Hydrogel Beads for Controlled Protein Release: Effect of PH and Crosslinking Agent. *J. Drug Deliv. Sci. Technol.* **2020**, *56*, 101551.

(34) Zhao, Y.; Li, F.; Carvajal, M. T.; Harris, M. T. Interactions between Bovine Serum Albumin and Alginate: An Evaluation of Alginate as Protein Carrier. *J. Colloid Interface Sci.* **2009**, *332* (2), 345–353.

(35) Loncaster, J. A.; Harris, A. L.; Davidson, S. E.; Logue, J. P.; Hunter, R. D.; Wycoff, C. C.; Pastorek, J.; Ratcliffe, P. J.; Stratford, I. J.; West, C. M. L. Carbonic Anhydrase (CA IX) Expression, a Potential New Intrinsic Marker of Hypoxia: Correlations with Tumor Oxygen Measurements and Prognosis in Locally Advanced Carcinoma of the Cervix. *Cancer Res.* **2001**, *61* (17), 6394–6399.

(36) Ikeda, E. Cellular Response to Tissue Hypoxia and Its Involvement in Disease Progression. *Pathol. Int.* **2005**, *55* (10), 603–610.

(37) Williams, K. J.; Gieling, R. G. Preclinical Evaluation of Ureidosulfamate Carbonic Anhydrase IX/XII Inhibitors in the Treatment of Cancers. *Int. J. Mol. Sci.* **2019**, *20* (23), 6080.

(38) Tripathi, V. K.; Subramaniyan, S. A.; Hwang, I. Molecular and Cellular Response of Co-Cultured Cells toward Cobalt Chloride (CoCl2)-Induced Hypoxia. *ACS Omega* **2019**, *4* (25), 20882–20893.

TOC graphic

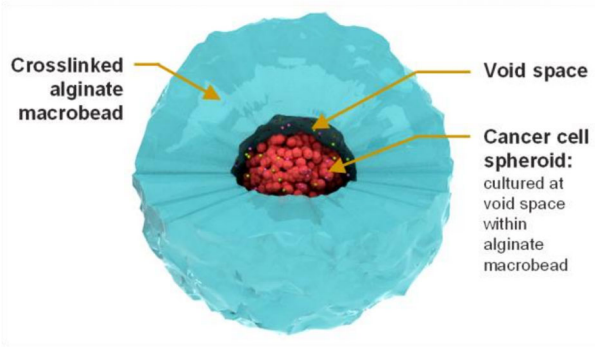
Crosslinked alginate macrobead
Void space
Cancer cell spheroid:
cultured at void space within alginate macrobead